LLNL-JRNL-440873

LAWRENCE
LIVERMORE
NATIONAL
LABORATORY

Principal Component Analysis of Multi Spectral Data for Near Real Time Skin Chromophore Mapping

J. M. Kainerstorfer, M. Ehler, F. Amyot, M. Hassan, S. G. Demos, V. Chernomordik, C. K. Hitzenberger, A. H. Gandjbakhche, J. D. Riley

May 25, 2010

Journal of Biomedical Optics

Disclaimer

This document was prepared as an account of work sponsored by an agency of the United States government. Neither the United States government nor Lawrence Livermore National Security, LLC, nor any of their employees makes any warranty, expressed or implied, or assumes any legal liability or responsibility for the accuracy, completeness, or usefulness of any information, apparatus, product, or process disclosed, or represents that its use would not infringe privately owned rights. Reference herein to any specific commercial product, process, or service by trade name, trademark, manufacturer, or otherwise does not necessarily constitute or imply its endorsement, recommendation, or favoring by the United States government or Lawrence Livermore National Security, LLC. The views and opinions of authors expressed herein do not necessarily state or reflect those of the United States government or Lawrence Livermore National Security, LLC, and shall not be used for advertising or product endorsement purposes.

Principal Component Analysis of Multi Spectral Data for Near Real Time Skin Chromophore Mapping

Jana M. Kainerstorfer[1, 2,*], Martin Ehler[3], Franck Amyot[4], Moinuddin Hassan[1], Stavros G. Demos[5], Victor Chernomordik[1], Christoph K. Hitzenberger[2], Amir H. Gandjbakhche[1] and Jason D. Riley[1]

1) National Institutes of Health, Eunice Kennedy Shriver National Institute of Child Health and Human Development, PPITS/SAFB, Bethesda, MD, 20892

2) Medical University of Vienna, Center for Medical Physics and Biomedical Engineering, Waehringer Str. 13, 1090 Vienna, Austria

3) National Institutes of Health, Eunice Kennedy Shriver National Institute of Child Health and Human Development, PPB/LIMB/SMB, Bethesda, MD, 20892

4) National Institutes of Health, National Institutes of Neurological Disorders and Stroke, Clinical Neuroscience Program, Bethesda, MD, 20892

5) Lawrence Livermore National Laboratory, Livermore, CA, 94551

* To whom all correspondence should be addressed

Jana Kainerstorfer
NIH/NICHD/PPITS/SAFB
9 Memorial Drive, Room B1E11
Bethesda, MD, 20982
301-594-0352; Fax: 301-480-2427
kainersj@mail.nih.gov

Keywords: multi-spectral imaging; tissue oxygenation; blood volume; Principal Component Analysis; modeling; biophotonics

Abstract

Multi-spectral images of skin contain information on the spatial distribution of biological chromophores, such as blood and melanin. From this, parameters such as blood volume and blood oxygenation can be retrieved using reconstruction algorithms. Most such approaches use some form of pixel-wise or volumetric reconstruction code. In this work we explore the use of Principal Component Analysis (PCA) of multi spectral images to access blood volume and blood oxygenation in near real time. We present data from healthy volunteers under arterial occlusion of the forearm, experiencing ischemia and reactive hyperemia. Using a two layered analytical skin model, we show reconstruction results of blood volume and oxygenation and compare it with the results obtained from our new spectral analysis based on Principal Component Analysis. We demonstrate that PCA applied to multi-spectral images gives near equivalent results for skin chromophore mapping and quantification with the advantage of being three orders of magnitude faster than the reconstruction algorithm.

Introduction

Assessing spatial distributions of skin chromophores such as blood and melanin can be achieved by diffuse multi-spectral imaging. Acquiring several wavelength images in the near infrared spectrum together with an analytical skin model, allows fitting the data to the model, thus extracting and mapping the spatial distribution of those parameters.

Diffuse multi spectral imaging of the skin and image reconstruction of skin chromophores has found its application in the clinic, successfully assessing parameters for healthy and diseased skin (1-7). Assessment of the metabolic state of skin surface lesions is often desired in clinical routines as a measure for treatment outcome. Near infrared diffuse multi-spectral imaging of the skin combined with an analytical, numerical, or stochastic skin model can provide this information by producing spatial maps of skin chromophore concentrations (5, 8, 9). The main parameters of interest are blood, melanin, lipids, and water, which exhibit separable absorption coefficients in the near infrared wavelengths range. The disadvantage of finding these parameters by fitting the data to an analytical skin model lies in the computationally expensive data post processing. This makes immediate conclusions difficult or even impossible if the image size is large, whereas in clinical routines it is often desired to assess the metabolic state of a tumor in real time. We are not aware of any current imaging protocol and reconstruction algorithm which can assess quantitative blood concentrations in real time.

Principal Component Analysis (PCA), first introduced in 1901 (10), is a statistical tool, which linearly transforms data into an orthogonal coordinate system, where the axes correspond to the inherent information within the data set. The idea is to reveal the data components (in a decreasing order) that best explain the variance in the data. PCA has

found applications in fields such as face recognition (11, 12), and image compression (13), and is a common technique for finding patterns in high dimensional data (14). It is further used for analyzing and visualizing gene expression data (15-17), for dimension reduction in hyperspectral imaging (18), as well as image enhancement (19). The main advantage of PCA is the speed of computation, which is in the order of seconds per image. For the biomedical optical imaging field, PCA found its place in various applications. The usage ranges from noise reduction and image enhancement (19) in multi spectral data for biological cell analysis (20) to pattern analysis for skin lesion classification (21). Applied to RGB images, PCA was used on relative color features for unsupervised lesion classification (22-24).

When imaging the skin in the visible light range, the dominant absorbing materials are blood and melanin and should therefore explain most of the variance in multi spectral data. Previous work by Tsumura et al. (25) showed that skin color in digital RGB images can be described by attributing melanin and blood to the first two principal components. Fadzil et al. (26, 27) used the same idea and applied PCA and Independent Component Analysis (ICA) to RGB data for blood and melanin extraction of vitiligo lesions to qualitatively evaluate the skin repigmentation progression.

In this work we evaluate the use of Principal Component Analysis (PCA) for retrieving quantitative near real time blood volume and blood oxygenation maps of skin areas of several square centimeters from a selected set of spectral images in the near infrared range (700 – 1000nm). Our experimental protocol involves imaging of healthy volunteers' lower forearm before, during, and after arterial occlusion. Occlusion

experiments were chosen, as the behavior of blood oxygenation is well known which is ischemia during and reactive hyperemia after release of pressure.

In the first part of the paper we describe the two layered analytical skin model used and show reconstruction results of blood volume and blood oxygenation over time. In the second part we apply PCA to the same data set and show that the first eigenvector correlates with blood volume and the second eigenvector with blood oxygenation. Finally we compare reconstruction results with the eigenvectors found by PCA and demonstrate the relationship between blood volume and the first eigenvector, as well as the relationship between blood oxygenation and the second eigenvector.

Materials

Instrumentation

The non-invasive, non-contact diffuse reflectance multi-spectral imaging system used in this work has been described in detail elsewhere (5) and shall only be described briefly here. Polarized light from a white light source (halogen 150W) is used for illumination of the sample. A second polarizer is placed before the detection unit, with its polarization orientation perpendicular to the incident beam polarization, thus guaranteeing diffuse reflectance measurements and removal of specular reflection (28).

Images are captured by a CCD camera (Princeton Instruments CCD-612-TKB, Roper Scientific) after passing consecutively one of six narrow bandpass filters (40nm FWHM, CVI Laser) on a filter wheel centered at 700, 750, 800, 850, 900 and 1000nm. For calibration purposes, images from a 90% reflectance paper (Kodak) are also acquired at each image filter.

Occlusion experiments on healthy volunteers

A pressure cuff was used to occlude the upper right arm of five right handed healthy volunteers with 180mmHg pressure. This amount of pressure was chosen to achieve arterial occlusion and the pressure lasted for 5min. Multi-spectral images were taken every 30 seconds before occlusion, during occlusion and for 5 minutes afterwards, resulting in 21 time points in total. Occlusion experiments were chosen as the behavior of blood volume and blood oxygenation over time is well known, which is ischemia during, and reactive hyperemia after occlusion (4, 8, 29, 30).

All volunteers signed a consent form approved by the Institutional Review Board of the Eunice Kennedy Shriver National Institute of Child Health and Human Development under the protocol number 08-CH-0001.

Methods

Reconstruction of skin chromophores

Diffuse multi-spectral images obtained during the occlusion experiment were used for reconstruction of blood volume and blood oxygenation. Preprocessing of the data included spectral and spatial illumination artifact removal as described in (5). The next step in preprocessing was rigid body registration for motion artifact removal and was performed by MultiStackReg in Image J. In a last step, curvature correction was performed to remove shape based intensity bias (31).

Four wavelength (λ) images were used (700, 750, 800, and 850nm) and reconstruction was performed using MATLAB (Math Works, Natick, MA) by least squares non linear fitting of the data to the analytical skin model used (5). The analytical skin model is based on a two layered structure, the first one being the melanin containing epidermis, the second one being the blood containing dermis, with optical properties of the skin taken from literature values (32-34), and can be written as:

$$I_e(\lambda) = S.A_e(\lambda)^2.A_d(\lambda) \qquad [1]$$

where I_e is the wavelength dependent intensity measured in the CCD camera. The attenuation by the epidermis, A_e, is based on Lambert's law and can be written as:

$$A_e(\lambda) = e^{-\mu_e.d_e} = e^{-\left(v_m \cdot 0.66 \cdot 10^{11} \cdot \lambda^{-3.33} \cdot d_e\right)} \qquad [2]$$

with v_m the concentration of melanin, d_e the thickness of the epidermis and μ_e the absorption coefficient of the epidermis, which is based on the absorption of melanin. The attenuation by the dermis, A_d, which includes the absorption due to blood volume, v_{db},

and oxygenation, v_{boxy}, is based on the analytical solution of photon migration in turbid media (35) based on random walk theory and can be written as:

$$A_d(\lambda) = \frac{e^{-2(\mu_d/\mu_s)}}{\sqrt{24(\mu_d/\mu_s)}} \cdot \left(1 - e^{-\sqrt{24(\mu_d/\mu_s)}}\right) \approx 1.06 - 1.45 \cdot (\mu_d/\mu_s)^{0.35} \quad [3]$$

$$\mu_d = v_{db} \cdot \left[(1 - v_{boxy}) \cdot \mu_{deoxy} + (v_{boxy}) \cdot \mu_{oxy}\right] \quad [4]$$

where μ_s is the reduced scattering coefficient and μ_d is the absorption coefficient of the dermis, with μ_{deoxy} and μ_{oxy} being the absorption coefficients of deoxygenated and oxygenated blood respectively. The scaling factor S, blood volume, v_{db}, and blood oxygenation, v_{boxy}, are unknown a priori and were solved for.

The scaling factor was calculated for each subject and time point and averaged over time. This so obtained subject specific scaling factor was then used to compute the 2D maps of blood volume and oxygenation over the course of the experiment. Computational time for each 2D image, which is in the order of 200 x 200 pixels, was 45min on a 2.6GHz, 3GB RAM Personal Computer (PC).

Principal Component Analysis

Principal Component Analysis (10) linearly transforms the data into an orthogonal coordinate system whose axes correspond to the principal components in the data, i.e., the first principal component accounts for as much variance in the data as possible and, successively, further components capture the remaining variance. Through an eigenanalysis, the principal components are determined as eigenvectors of the dataset's covariance matrix and the corresponding eigenvalues refer to the variance that is captured within each eigenvector.

We use three wavelengths (750, 800, 850nm) from the occlusion experiment, which provides three 2D images. These wavelengths were chosen, as they are centered around 800nm, which is the isosbestic point of blood, where the absorption coefficient of deoxygenated (Hb) and oxygenated (HbO2) blood are equal. Fig. 1 shows the absorption spectra for Hb and HbO2, illustrating that the absorption of Hb is dominant at 750nm and for HbO2 at 850nm. In this wavelength range, the dominant chromophore is blood and should therefore explain most of the variance of the data.

After subtracting the mean of the data, PCA was performed on the collection of three-dimensional pixel vectors $\{x_1,...,x_n\}$ of the zero mean data. We first diagonalize the covariance matrix

$$Cov(X) = E(XX^T), \qquad [5]$$

where $X = (x_1, .. x_n)$ is the zero mean data matrix. The three eigenvectors p_1, p_2, p_3 - the principal components ordered according to the magnitude of their eigenvalues – provide the transformed data

$$Y = W^T X, \qquad [6]$$

where $W = (p_1 \quad p_2 \quad p_3)$. Rearranging the vectors in Y into matrices yields again three 2D images. The first image represents the projected data along the first eigenvector. As mentioned above, blood is the dominant chromophore, and it will turn out that the first layer correlates with blood volume. The second image is each datapoint's projection along the second eigenvector and we will show that it correlates with blood oxygenation.

The computational time to process one set of data (three images at 21 timepoints) on a 2.6GHz, 3GB RAM PC was in the order of 1 second.

Results

In order to evaluate the potential of PCA to retrieve the spatial distribution of chromophores, we first generate a conventional pixel-wise reconstruction of blood volume and oxygenation over an imaging area of several centimeters. We then compare results after applying PCA to the contributions of the principal components. The objective was to demonstrate the anticipated response (ischemia and reactive hyperemia) for all subjects and a qualitative and quantitative assessment of the consistency between reconstruction results and the eigenvectors.

Fig. 2 shows 2D reconstruction maps of fractional blood volume concentrations over time for one representative healthy volunteer's lower forearm. Only every second time point is shown for conciseness, with the first row showing the baseline before occlusion, row 2 and 3 showing results during and after occlusion respectively. Veins contain more blood than the surrounding tissue and are clearly separable in the reconstruction maps by increased blood volume. Fig. 3 shows the corresponding blood oxygenation result over time, before, during, and after occlusion. Veins do not show a significant difference in blood oxygenation compared to surrounding tissue and can not be easily separated. The overall tissue oxygenation follows the typical expected trend of ischemia during occlusion (drop of oxygenation compared to baseline) and reactive hyperemia after occlusion (over shoot compared to baseline).

To evaluate the ischemic and hyperemic behavior even further, average concentrations of blood volume and oxygenation were calculated over the entire 2D maps for each time point. The results for four subjects can be seen in Fig. 4a for blood volume and 4b for

blood oxygenation, with error-bars given by the standard deviation over all pixels per time point. Only four of the five subjects were included in the analysis, as the analysis of the fifth subject was hindered by motion artifacts greater than one third of the image size. The dashed lines indicate the time points of beginning and ending of applied pressure. Fig. 4a shows that blood volume stays over time within 5% variation, while Fig. 4b shows changes in blood oxygenation over time, corresponding to ischemia during and reactive hyperemia after occlusion.

Fig. 5 shows a set of three wavelength images (750, 800, 850nm), represented in a 3D scatter-plot in the wavelength space, with each pixel being color-coded by the reconstruction results of blood volume (Fig. 5a) and blood oxygenation (Fig. 5b). Data shown in this figure are from the same subject as in Fig. 2 and Fig. 3 at the 12th time point, which is the first point after occlusion. All other subjects and time points show a similar behavior, which can be summarized as following: a) the data is of elliptical distribution, indicating that it can be described by a linear transformation. b) The reconstruction values of blood volume lay along the main axis of the ellipse, which will be described as eigenvector 1 (vertical black line in Fig. 5a and Fig. 5b), and are well separable. c) The reconstruction results of blood oxygenation show a separation perpendicular to the main axis of the ellipse, which will be described as eigenvector 2 (horizontal black line in Fig. 5a and Fig. 5b). All three points combined indicate that a linear transform of the data by PCA is not only valid, but that it should be possible to separate blood volume and oxygenation. The separation between blood volume and oxygenation with PCA can only be possible, if alignment perpendicular to each other is

given. This is an inherent necessity for PCA, since data is being described with eigenvectors, which are perpendicular to each other.

We subsequently performed PCA for each set of wavelength images and time points for all subjects. Doing so, we obtained three eigenvectors per time point and subject. Eigenvector 1 was found to be the same for each subject and over all 21 time points, except for small angular shifts (data not shown), and being well aligned with blood volume (see Fig. 5a). Stability over time and subjects in eigenvector 1 indicates reliability in calculation. Eigenvector 2 and 3 showed large deviations within one subject and no consistent pattern was found over time, indicating that the separation between eigenvector 2 and 3 was ambiguous. An ambiguity in eigenvector 2 and 3 indicates that blood volume and oxygenation can not be reliably separated. Neither eigenvector 2 nor 3 showed any temporal change similar to blood oxygenation over time. Fig. 6a demonstrates this non specific behavior, showing a transformed data set along the 2nd and 3rd eigenvector, color-coded by blood oxygenation. Data shown here is from the same subject as in Fig. 5, but at different time point. As the apparent structure of the oxygenation results is not aligned with either eigenvector, PCA failed to attribute one specific direction to blood oxygenation when performed on one single data set of three wavelength images.

The blood oxygenation color-coded data appeared aligned and perpendicular to the primary axis of the ellipse when looking at each time point separately. The next step in the analysis was therefore to create one large data set per subject, which included all time points (21 times 3 wavelength images) and resulted into one set of eigenvectors per subject. Fig. 6b shows the result of the same subject for the large data set color-coded by

blood oxygenation. The data are well aligned along the second eigenvector with blood oxygenation values being aligned in the same direction, therefore showing a dependence of the 2nd eigenvector on oxygenation. Fig. 6c shows the same data as in Fig. 6a (one time point) but transformed with the eigenvectors found by the data set including all time points. When applying the subject specific eigenvector set, the data and its oxygenation become aligned to the second eigenvector. This phenomenon is consistent for all subjects and time points, making it possible to separate blood volume and oxygenation .

In Fig. 7 we demonstrate the validity of image summation (creating a single data set for all time points) for PCA analysis. Here we assume that the set of 21 images is sufficient to develop a patient specific component space. We plot 'n' against angular offset of the eigenaxes, where n is the number of images used to generate the PCA summation space. For each n we generate 100 random choices of images (note that duplication occurs only for n=1 and n=21). Fig. 7a shows the plot of average angular separation of an individual summation space from the average space (21 images), with standard deviation for eigenvector 1 (data in blue). The separation of the final angular eigensystem from ground truth (given as the eigensystem of the entire image ensemble) is also shown (data in red). Fig. 7b and Fig. 7c show the same data for eigenvectors 2 and 3.

Fig. 8 shows the 2D representation of the transformed data along the three eigenvectors over time for the same subject as in Fig. 2 and Fig. 3. The eigenvectors used were obtained by taking a combined data set of all time points per subject. Fig. 8a shows the result for the first eigenvector, which shows the same structures and temporal behavior as blood volume in Fig. 2. Eigenvector 2 can be seen in Fig. 8b, which shows a similar temporal and spatial appearance as blood oxygenation, as seen in Fig. 3. Fig. 8c shows

eigenvector 3, which does not show significant trends or structures and might be attributed to noise. It shall be mentioned that the scales in the three images is different from each other and that the first eigenvector is one magnitude larger than eigenvector 2 and 3.

Results in Fig. 9 show the average distances along the eigenvectors. The average was taken as in Fig. 4 over the entire 2D maps for each time point, with error-bars given by the standard deviation over all pixels per time point. The qualitative behavior over time for eigenvector 1 (9a) matches the behavior seen in Fig. 4a; eigenvector 2 (9b) shows the same temporal behavior as Fig. 4b. Combined with the results from Fig. 5 and Fig. 6, the data suggest that the first eigenvector can be described by blood volume and the second one by blood oxygenation. The third eigenvector (9c) does not show any change over time.

Fig. 10a shows the direct comparison between eigenvector 1 and blood volume and 10b between eigenvector 2 and blood oxygenation for all pixels and time points per subject. A clear almost linear relationship can be seen between eigenvector 1 and blood volume, indicating that these two are uniquely correlated. The same trend can be seen for all subjects, but subject 3 shows a shift towards higher blood volume values. Fig. 10b shows the results for eigenvector 2 versus blood oxygenation. The relationship is not as linear but blurred compared to 10a, as well as shifted along the eigenvector axis. This indicates that blood oxygenation values can be recovered within a constant shift compared to reconstruction results.

Discussion

Diffuse multi spectral imaging of skin in the near infrared wavelength range allows for quantitative chromophore assessment which can be used to attain functional information. Especially blood volume and oxygenation are of interest for skin lesion treatment follow up as a parameter of the angeogenic process and metabolic state of a tumor. Previous work of assessing these parameters in healthy and diseased skin (1-9) included fitting the acquired intensity data to an analytical model of photon migration in diffuse media. Reconstructed concentration maps are therefore based on the wavelength dependent absorption coefficient and require an accurate model. Furthermore, model based reconstruction is computationally intense and time consuming, therefore not applicable for real time assessment in a clinical setting.

PCA has been used as a tool to analyze digital RGB images for extracting blood and melanin concentration and for lesion segmentation in various conditions (21-25). To our best knowledge, no attempt was done for extraction of blood oxygenation using PCA from RGB or multispectral images or for comparison of PCA with reconstruction results.

The reconstruction results of four healthy volunteers undergoing occlusion of the upper arm and imaged at the forearm (Fig. 2-4) presented in this work demonstrate that the spatial distribution (Fig. 8) and temporal behavior (Fig. 9) of eigenvector 1 matches that of blood volume and eigenvector 2 matches that of blood oxygenation. In order to obtain these results, one data set, including all time points per subjects, was created, as we have seen that PCA does not pick up on blood oxygenation otherwise. Surprisingly the subject specific eigenvector set is the same for all four subjects with only small angular shifts smaller than 7 degree (data not shown). This overlap in eigenvectors indicates that it

might be possible to create one general set of eigenvectors describing blood volume and oxygenation. This of course raises the question if such a description is valid when applied to a different data set, i.e. from skin lesions, and if the transformation still holds. In addition, arterial blood could not be imaged, as arteries lie deeper in the skin. It would be of interest to validate the PCA results with arterial oxygenation values, which are in the order of 99%. Future work will be addressing these questions.

The results also indicate an almost linear dependence of the first eigenvector with blood volume (Fig. 10a), demonstrating that values from PCA can be converted to actual concentrations of blood volume. Only subject 3 showed a deviation from the others in terms of a shift towards higher values of blood volume. This shift might be explained by the nature of our reconstruction algorithm, which assumes the same epidermal thickness for all subjects' forearms (60µm). We have data (unpublished) which shows that a difference of the epidermal thickness within the standard deviation of reported literature values for arms will lead to a significant overestimation of blood volume. The shift in Fig. 10a can therefore be explained by the inaccuracy of the reconstruction rather than due to PCA errors.

Fig. 10b indicates that there is a defined relationship between eigenvector 2 and blood oxygenation, but it is much more blurred and shifted along the eigenaxis. We hypothesize that the blurring might be partially explained by reconstruction errors of blood oxygenation as well as PCA itself. As mentioned above, PCA applied to one single image did not successfully align the axis of oxygenation changes to one specific eigenaxis and a data set including all time points was required to do so. The data was therefore centered on the mean of the large data set, not the individual ones. As the second principal

component is one order of magnitude smaller than the first component, even small shifts in the data over time will lead to relatively larger errors (blurring) compared to the first component. The shift along the second eigenvector, in particular for subject 2 (Fig. 10b), might well be explained by centering the large data set rather than the individual ones. When transforming the data with a given set of eigenvectors, the resulting data is not necessarily centered on the origin, leading to shifts along the axes.

The results from the direct comparison between reconstruction of blood volume and oxygenation with the PCA results of the same multi-spectral image set indicates that PCA may be a viable alternative tool for skin chromophore assessment. Future work will have to include phantom experiments as well as skin structure assessment for improvement of the reconstruction results and thus explaining remaining variation in the direct comparison between PCA and reconstruction results. Since PCA is considerably faster (three orders of magnitude) compared to the time consuming reconstruction algorithms commonly used, it may provide a significant advantage for extracting metabolic information results in real time. Future work will include applying PCA to multi spectral data from skin surface lesions, as well as acquiring more data from healthy volunteers to increase statistical power.

Conclusion

We acquired multi spectral images from healthy volunteers' lower forearms during an occlusion experiment and compared reconstruction results for blood oxygenation and blood volume with results from PCA. Reconstruction was performed by fitting the data to our two layered analytical skin model and blood oxygenation results showed the expected course of ischemia during occlusion and reactive hyperemia afterwards. PCA was performed on a large data set of all time points per subject and one subject specific set of eigenvectors was used to transform the time dependent data. Results showed that the first principal component corresponds well to the time course and spatial distribution of blood volume, the second one to blood oxygenation, and the third one did not show any temporal or spatial change. A direct comparison between reconstruction results and principal components showed a linear dependence between blood volume and blood oxygenation with the first and second component respectively. The correspondence between blood oxygenation and the second principal component was blurred and a shift between subjects was observed, indicating that the dependence is more susceptible to noise and errors. The results are encouraging and demonstrate the potential of PCA for quantitative skin chromophore assessment. The biggest advantage of PCA compared to reconstruction algorithms is its computational inexpensiveness, with PCA being three orders of magnitude faster. This allows for real time mapping of skin chromophores with PCA and would therefore find great use in clinical routines.

This work performed under the auspices of the U.S. Department of Energy by Lawrence Livermore National Laboratory under Contract DE-AC52-07NA27344.

1. S. L. Jacques, J. C. Ramella-Roman and K. Lee, "Imaging skin pathology with polarized light," Journal of biomedical optics 7(3), 329-340 (2002)

2. G. Mantis and G. Zonios, "Simple two-layer reflectance model for biological tissue applications," Appl Opt 48(18), 3490-3496 (2009)

3. Y. Miyamae, Y. Yamakawa, M. Kawabata and Y. Ozaki, "A noninvasive method for assessing interior skin damage caused by chronological aging and photoaging based on near-infrared diffuse reflection spectroscopy," Appl Spectrosc 62(6), 677-681 (2008)

4. S. H. Tseng, P. Bargo, A. Durkin and N. Kollias, "Chromophore concentrations, absorption and scattering properties of human skin in-vivo," Opt Express 17(17), 14599-14617 (2009)

5. A. Vogel, V. V. Chernomordik, J. D. Riley, M. Hassan, F. Amyot, B. Dasgeb, S. G. Demos, R. Pursley, R. F. Little, R. Yarchoan, Y. Tao and A. H. Gandjbakhche, "Using noninvasive multispectral imaging to quantitatively assess tissue vasculature," Journal of biomedical optics 12(5), 051604 (2007)

6. C. Zakian, I. Pretty, R. Ellwood and D. Hamlin, "In vivo quantification of gingival inflammation using spectral imaging," Journal of biomedical optics 13(5), 054045 (2008)

7. M. Attas, M. Hewko, J. Payette, T. Posthumus, M. Sowa and H. Mantsch, "Visualization of cutaneous hemoglobin oxygenation and skin hydration using near-infrared spectroscopic imaging," Skin Res Technol 7(4), 238-245 (2001)

8. J. Kainerstorfer, F. Amyot, S. G. Demos, M. Hassan, V. Chernomordik, C. K. Hitzenberger, A. H. Gandjbakhche and J. D. Riley, "Quantitative assessment of ischemia and reactive hyperemia of the dermal layers using multi - Spectral imaging on the human

arm," Progress in Biomedical Optics and Imaging - Proceedings of SPIE 7369(no. 73690P), (2009)

9. A. Vogel, B. Dasgeb, M. Hassan, F. Amyot, V. Chernomordik, Y. Tao, S. G. Demos, K. Wyvill, K. Aleman, R. Little, R. Yarchoan and A. H. Gandjbakhche, "Using quantitative imaging techniques to assess vascularity in AIDS-related Kaposi's sarcoma," Conf Proc IEEE Eng Med Biol Soc 1(232-235 (2006)

10. K. Pearson, "On lines and planes of closest fit to systems of points in space," Philosophical Magazine 2((1901)

11. H. Moon and P. J. Phillips, "Computational and performance aspects of PCA-based face-recognition algorithms," Perception 30(3), 303-320 (2001)

12. M. Turk and A. Pentland, "Eigenfaces for recognition," Journal of Cognitive Neuroscience 3(1), 71-86 (1991)

13. Q. Du and J. E. Fowler, "Low-complexity principal component analysis for hyperspectral image compression," International Journal of High Performance Computing Applications 22(438 (2008)

14. A. Ferraz, E. Esposito, R. E. Bruns and N. DurÃ¡n, "The use of principal component analysis (PCA) for pattern recognition in Eucalyptus grandis wood biodegradation experiments," World Journal of Microbiology and Biotechnology 14(4), 487-490 (1998)

15. J. R. de Haan, R. Wehrens, S. Bauerschmidt, E. Piek, R. C. van Schaik and L. M. C. Buydens, "Interpretation of ANOVA models for microarray data using PCA," Bioinformatics 23(2), 184-190 (2007)

16. K. Nishimura, K. Abe, S. Ishikawa, S. Tsutsumi, K. Hirota, H. Aburatani and M. Hirose, "A PCA Based Method of Gene Expression Visual Analysis," Genome Informatics 14(346 (2003)

17. B. Sghaier-Hammami, L. Valledor, N. Drira and J. V. Jorrin-Novo, "Proteomic analysis of the development and germination of date palm [Phoenix dactylifera L.) zygotic embryos," Proteomics 9(9), 2543-2554 (2009)

18. G. Begelman, M. Zibulevsky, E. Rivlin and T. Kolatt, "Blind decomposition of transmission light microscopic hyperspectral cube using sparse representation," IEEE Transactions on Medical Imaging 28(8), 1317-1324 (2009)

19. H. Mandelkow, D. Brandeis and P. Boesiger, "Good practices in EEG-MRI: The utility of retrospective synchronization and PCA for the removal of MRI gradient artefacts," NeuroImage 49(3), 2287-2303 (2010)

20. L. L. Nuffer, P. A. Medvick, H. P. Foote and J. C. Solinsky, "Multispectral/hyperspectral image enhancement for biological cell analysis," Cytometry A 69(8), 897-903 (2006)

21. Z. She, Y. Liu and A. Damatoa, "Combination of features from skin pattern and ABCD analysis for lesion classification," Skin Res Technol 13(1), 25-33 (2007)

22. Y. Cheng, R. Swamisai, S. E. Umbaugh, R. H. Moss, W. V. Stoecker, S. Teegala and S. K. Srinivasan, "Skin lesion classification using relative color features," Skin Res Technol 14(1), 53-64 (2008)

23. G. Hance, S. E. Umbaugh, R. H. Moss and W. V. Stoecker, "Unsupervised Color Image Segmentation," IEEE Eng in Medicine and Biology 96((1996)

24. S. E. Umbaugh, R. H. Moss, W. V. Stoecker and G. Hance, "Automatic Color Segmentation Algorithms," IEEE Eng in Med Bio 93((1993)

25. N. Tsumura, H. Haneishi and Y. Miyake, "Independent-component analysis of skin color image," J Opt Soc Am A Opt Image Sci Vis 16(9), 2169-2176 (1999)

26. M. H. Fadzil, S. Norashikin, H. H. Suraiya and H. Nugroho, "Independent component analysis for assessing therapeutic response in vitiligo skin disorder," Journal of medical engineering & technology 33(2), 101-109 (2009)

27. H. Nugroho, M. H. Fadzil, V. V. Yap, S. Norashikin and H. H. Suraiya, "Determination of skin repigmentation progression," Conf Proc IEEE Eng Med Biol Soc 2007(3442-3445 (2007)

28. S. G. Demos and R. R. Alfano, "Optical polarization imaging," Applied Optics 36(1), 150-155 (1997)

29. D. J. Cuccia, F. Bevilacqua, A. J. Durkin, F. R. Ayers and B. J. Tromberg, "Quantitation and mapping of tissue optical properties using modulated imaging," Journal of biomedical optics 14(2), 024012 (2009)

30. U. Merschbrock, J. Hoffmann, L. Caspary, J. Huber, U. Schmickaly and D. W. Lubbers, "Fast wavelength scanning reflectance spectrophotometer for noninvasive determination of hemoglobin oxygenation in human skin," International journal of microcirculation, clinical and experimental / sponsored by the European Society for Microcirculation 14(5), 274-281 (1994)

31. J. Kainerstorfer, F. Amyot, M. Ehler, M. Hassan, S. G. Demos, V. Chernomordik, C. K. Hitzenberger, A. H. Gandjbakhche and J. D. Riley, "Direct Curvature Correction

for Non-Contact Imaging Modalities – Applied to Multi-Spectral Imaging," Journal of biomedical optics in review((2010)

32. S. L. Jacques, "Skin Optics," Oregon Medical Laser Center News <http://omlc.ogi.edu/news/jan98/skinoptics.html>((1998)

33. I. V. Meglinski and S. J. Matcher, "Quantitative assessment of skin layers absorption and skin reflectance spectra simulation in the visible and near-infrared spectral regions," Physiol Meas 23(4), 741-753 (2002)

34. S. Prahl, "Skin Optics," Oregon Medical Laser Center News <http://omlc.ogi.edu/spectra/hemoglobin/index.html>((1998)

35. A. H. Gandjbakhche and G. H. Weiss, "Random walk and diffusion-like models of photon migration in turbid media," Progress in Optics XXXIV(V), 335-402 (1995)

Figure Legend

Figure 1 Absorption spectra of deoxygenated (Hb) and oxygenated (HbO2) blood with the isosbestic point of blood at 800nm. For 750nm and 850nm, the absorption coefficients for oxygenated and deoxygenated blood are well separable.

Figure 2 Fractional blood volume concentrations over time. The first row shows the reconstructed blood volume map over several centimeters of a lower forearm before occlusion. The second row shows blood volume of the same area of the arm during occlusion and the third row shows results after release of pressure. Veins are clearly distinguishable due to the increase in blood compared to surrounding tissue.

Figure 3 Fractional blood oxygenation over time of the same area as shown in figure 1. The second row shows blood oxygenation during occlusion and the expected ischemic behavior, which is a decrease in oxygenated blood. The third row shows the expected hyperemic behavior, which is an overshoot of oxygenation.

Figure 4 Average Blood Volume (4a) and Blood Oxygenation (4b) over time for four subjects. The dashed lines indicate start and end of occlusion.

Figure 5 3D scatterplots of wavelength specific intensity data colorcoded with a) blood volume and b) blood oxygenation. The black lines indicate the eigenaxes found by PCA. Eigenvector 1 is aligned with blood volume, eigenvector 2 with blood oxygenation.

Figure 6 Transformed data after PCA in the eigenvector 2 and 3 plane, color-coded with the corresponding blood oxygenation results. 6a shows PCA performed on one time point, 6b over the data including all time points, and 6c shows the transformed data of one time point using the set of eigenvectors obtained in 6b.

Figure 7 Validity of image summation for PCA. Data in blue is average distance from local ensemble plus its standard deviation. Data in red is distance of local ensemble average from 'truth' (21 image ensemble). Fig. 7a shows data from eigenvector 1; 7b from eigenvector 2; and 7c from eigenvector 3.

Figure 8 Eigenvectors obtained by PCA over time for one subject. 8a shows the first eigenvector, which corresponds to blood volume; 8b shows the second eigenvector, which corresponds to blood oxygenation; 8c shows the third eigenvector.

Figure 9 Average eigenvectors over time for four subjects. The dashed lines indicate start and end of occlusion. Fig. 9a shows eigenvector 1, 9b eigenvector 2, 9c eigenvector 3.

Figure 10 Blood volume vs. eigenvector 1 (10a) and Blood oxygenation vs. eigenvector 2 (10b).

Figure 1

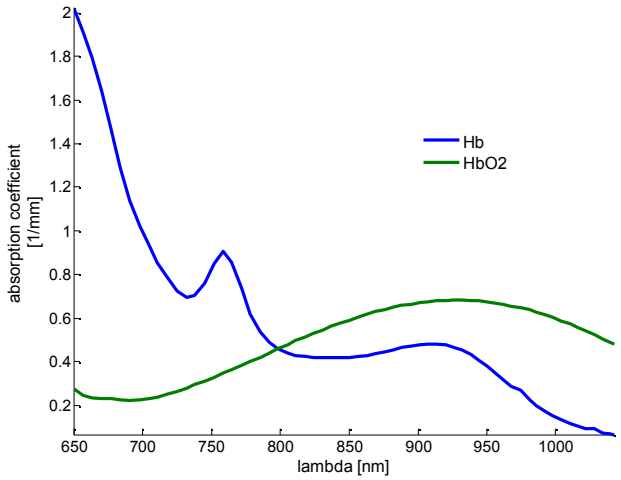
absorption coefficient
[1/mm]
lambda [nm]
Hb
HbO2
2
1.8
1.6
1.4
1.2
1
0.8
0.6
0.4
0.2
650
700
750
800
850
900
950
1000

Figure 2

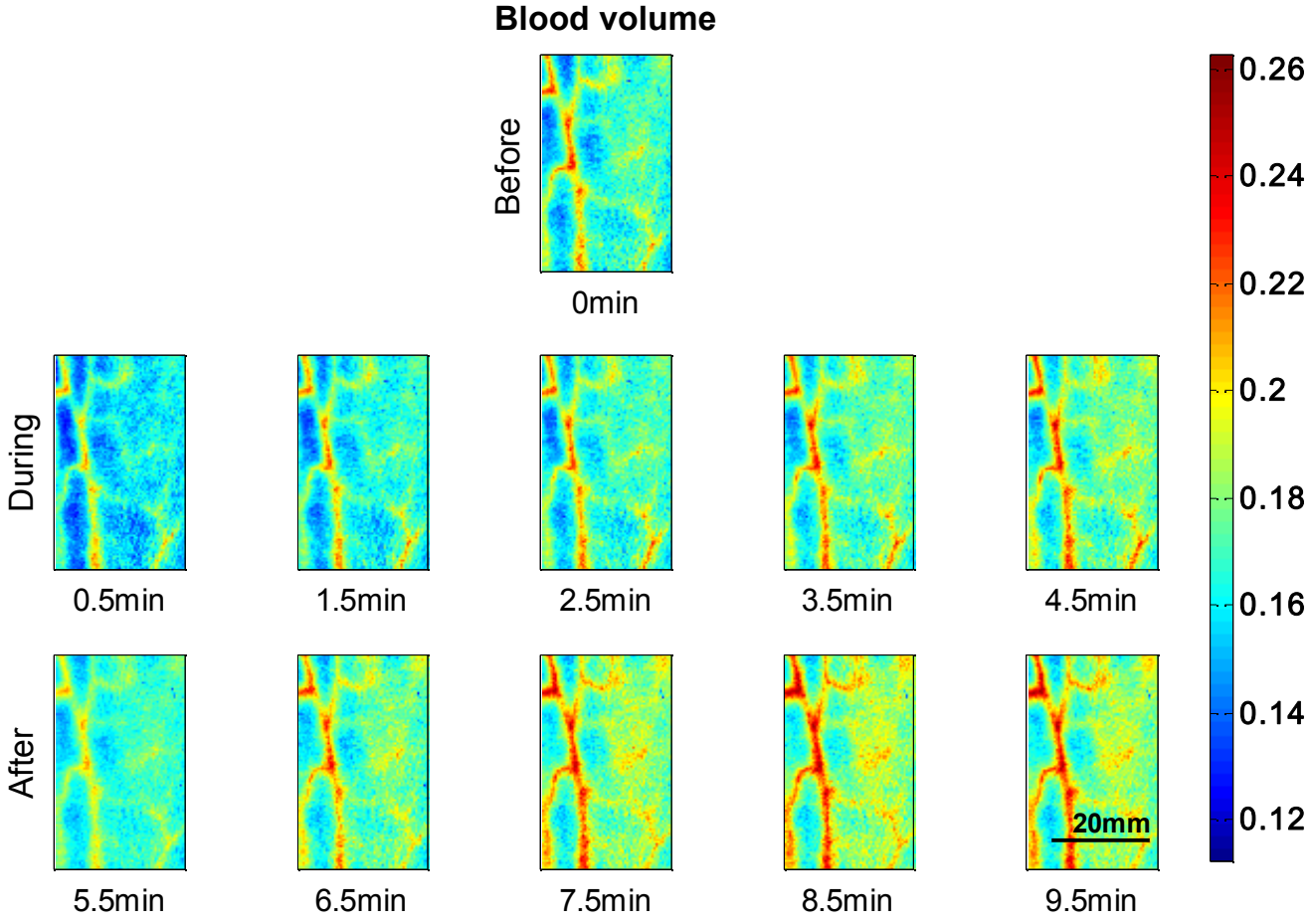
Blood volume
Before
0min
During
0.5min
1.5min
2.5min
3.5min
4.5min
After
5.5min
6.5min
7.5min
8.5min
9.5min
20mm
0.26
0.24
0.22
0.2
0.18
0.16
0.14
0.12

Figure 3

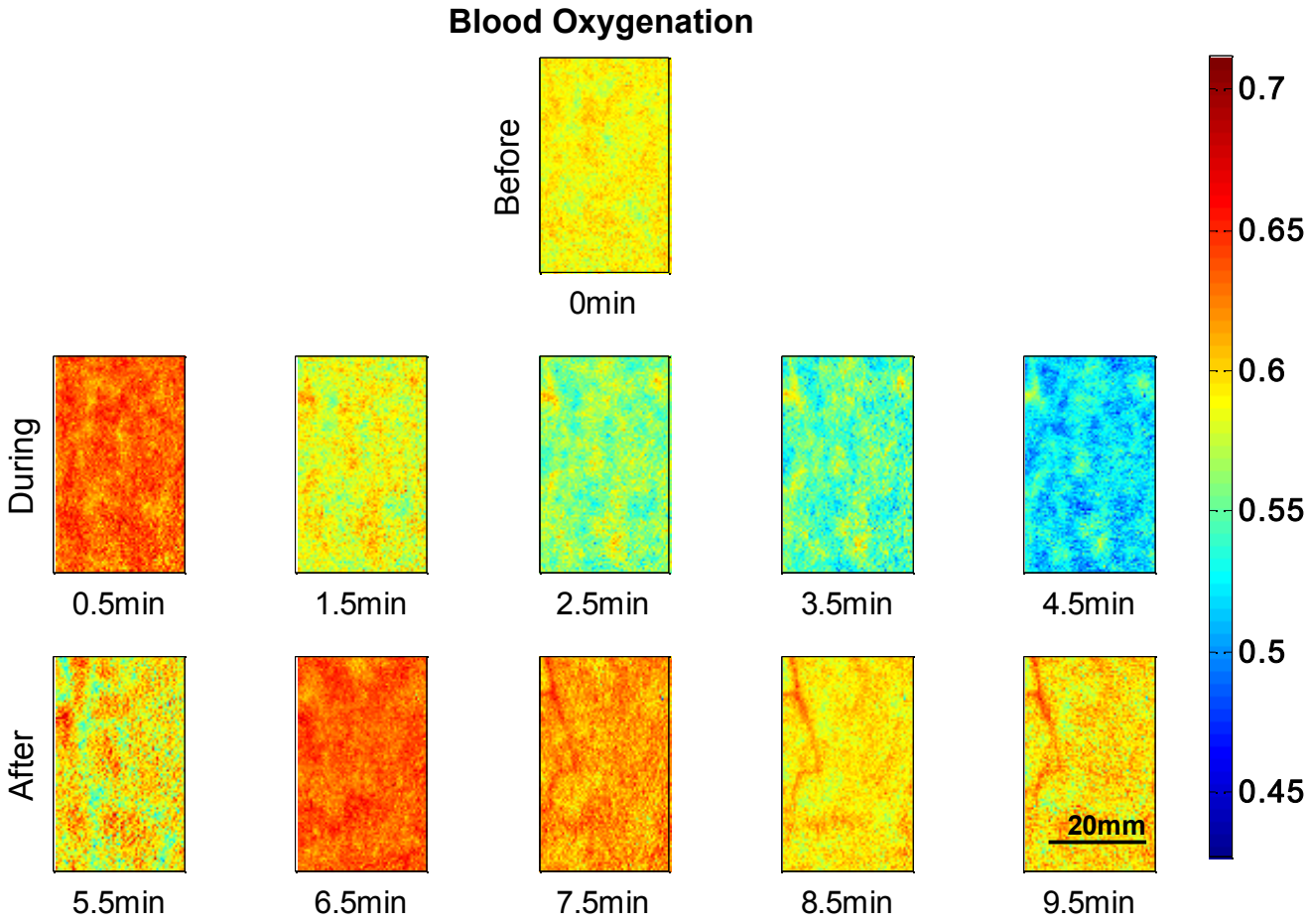
Blood Oxygenation
Before
0min
During
0.5min
1.5min
2.5min
3.5min
4.5min
After
5.5min
6.5min
7.5min
8.5min
9.5min
20mm
0.7
0.65
0.6
0.55
0.5
0.45

Figure 4

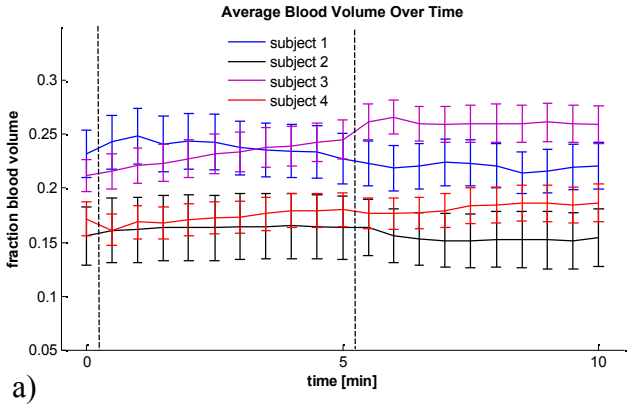
Average Blood Volume Over Time
subject 1
subject 2
subject 3
subject 4
fraction blood volume
0.05
0.1
0.15
0.2
0.25
0.3
0
5
10
time [min]

a)

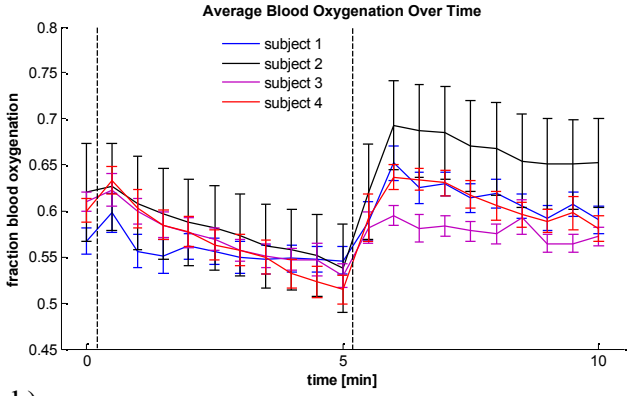
Average Blood Oxygenation Over Time
subject 1
subject 2
subject 3
subject 4
fraction blood oxygenation
0.45
0.5
0.55
0.6
0.65
0.7
0.75
0.8
0
5
10
time [min]

b)

Figure 5

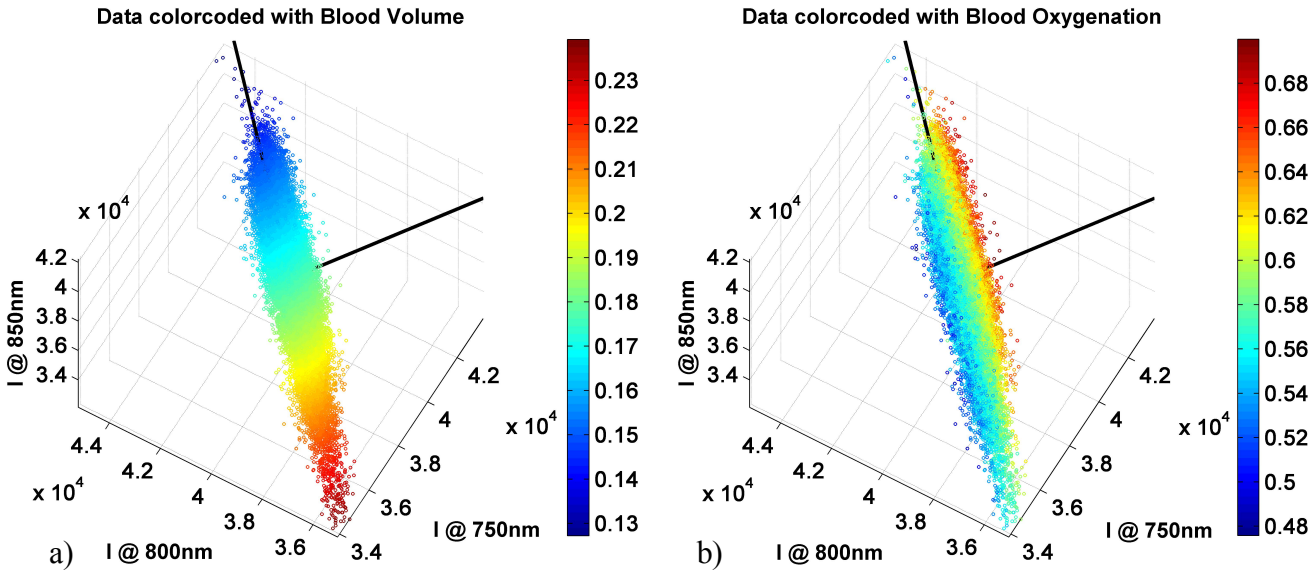
Data colorcoded with Blood Volume
x 10^4
I @ 850nm
4.2
4
3.8
3.6
3.4
4.4
4.2
4
3.8
3.6
x 10^4
I @ 800nm
4.2
4
3.8
3.6
3.4
x 10^4
I @ 750nm
0.23
0.22
0.21
0.2
0.19
0.18
0.17
0.16
0.15
0.14
0.13
a)
Data colorcoded with Blood Oxygenation
x 10^4
I @ 850nm
4.2
4
3.8
3.6
3.4
4.4
4.2
4
3.8
3.6
x 10^4
I @ 800nm
4.2
4
3.8
3.6
3.4
x 10^4
I @ 750nm
0.68
0.66
0.64
0.62
0.6
0.58
0.56
0.54
0.52
0.5
0.48
b)

Figure 6

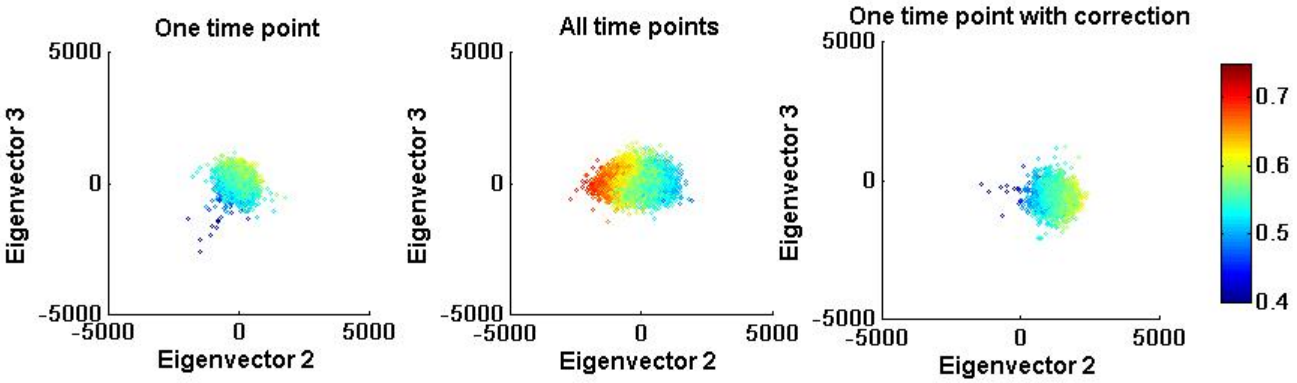
One time point
All time points
One time point with correction
Eigenvector 3
Eigenvector 2
5000
0
-5000
0.7
0.6
0.5
0.4

a) b) c)

Figure 7

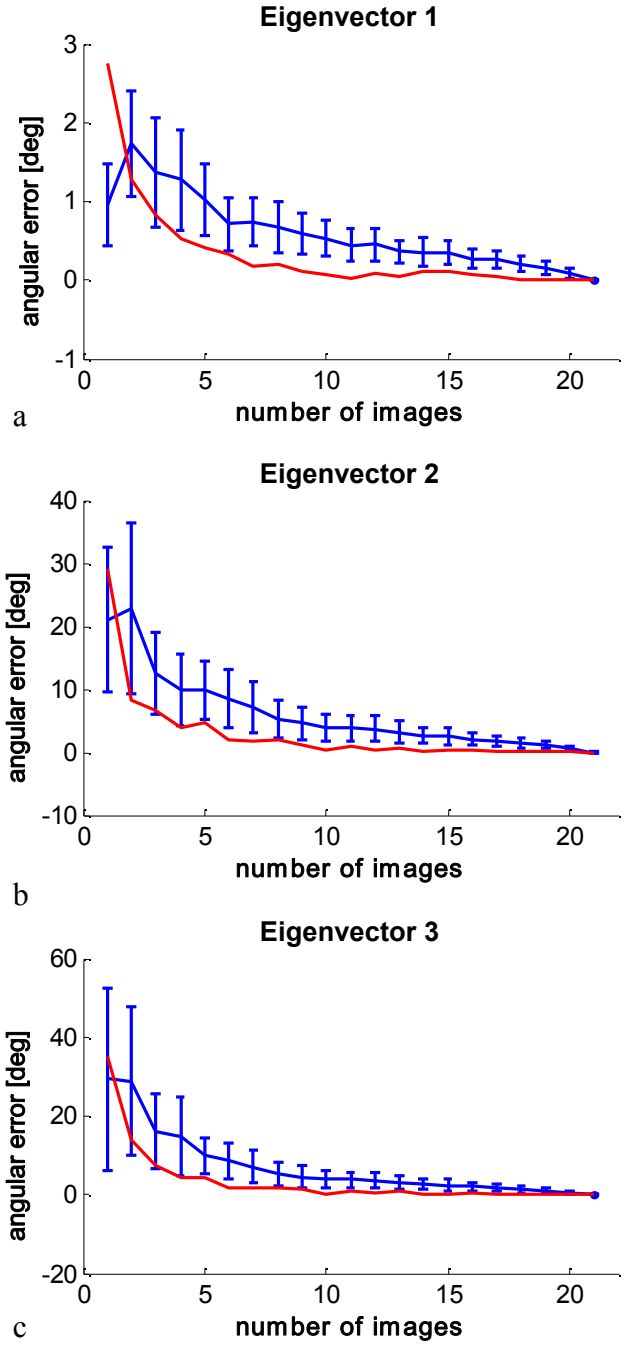
Eigenvector 1
angular error [deg]
number of images
a
Eigenvector 2
angular error [deg]
number of images
b
Eigenvector 3
angular error [deg]
number of images
c

Figure 8

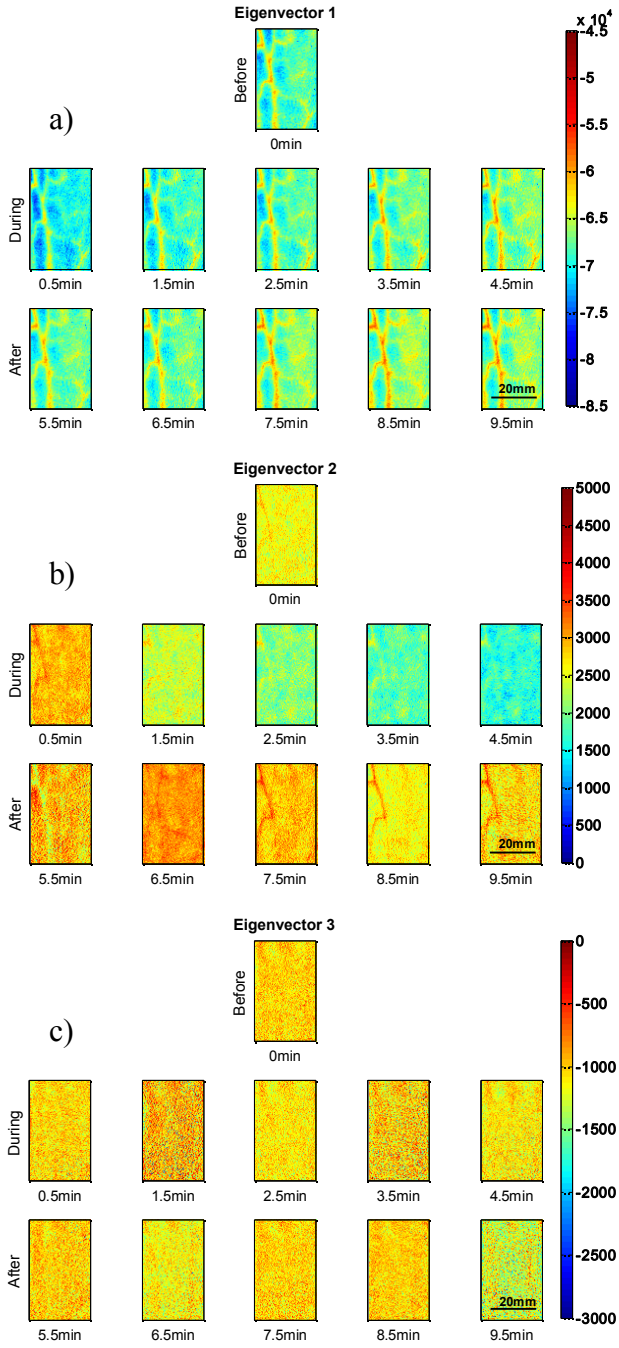
a)
Eigenvector 1
x 10^4
Before
0min
During
0.5min
1.5min
2.5min
3.5min
4.5min
After
5.5min
6.5min
7.5min
8.5min
9.5min
20mm
-4.5
-5
-5.5
-6
-6.5
-7
-7.5
-8
-8.5
b)
Eigenvector 2
Before
0min
During
0.5min
1.5min
2.5min
3.5min
4.5min
After
5.5min
6.5min
7.5min
8.5min
9.5min
20mm
5000
4500
4000
3500
3000
2500
2000
1500
1000
500
0
c)
Eigenvector 3
Before
0min
During
0.5min
1.5min
2.5min
3.5min
4.5min
After
5.5min
6.5min
7.5min
8.5min
9.5min
20mm
0
-500
-1000
-1500
-2000
-2500
-3000

Figure 9

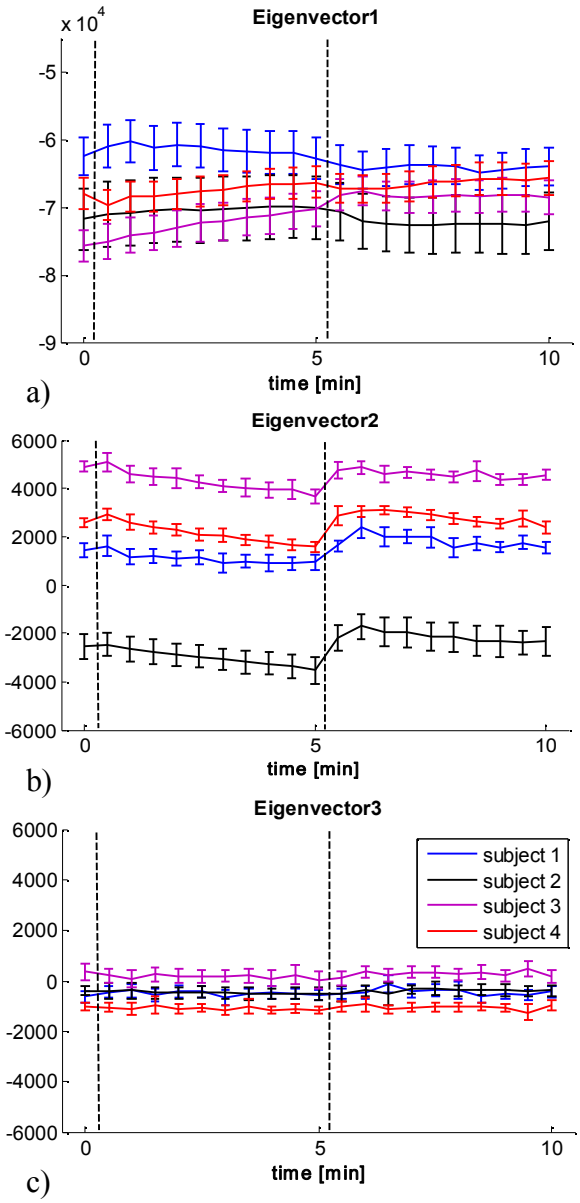
x 10^4
Eigenvector1
-5
-6
-7
-8
-9
0
5
10
time [min]
a)
Eigenvector2
6000
4000
2000
0
-2000
-4000
-6000
0
5
10
time [min]
b)
Eigenvector3
6000
4000
2000
0
-2000
-4000
-6000
0
5
10
time [min]
subject 1
subject 2
subject 3
subject 4
c)

Figure 10

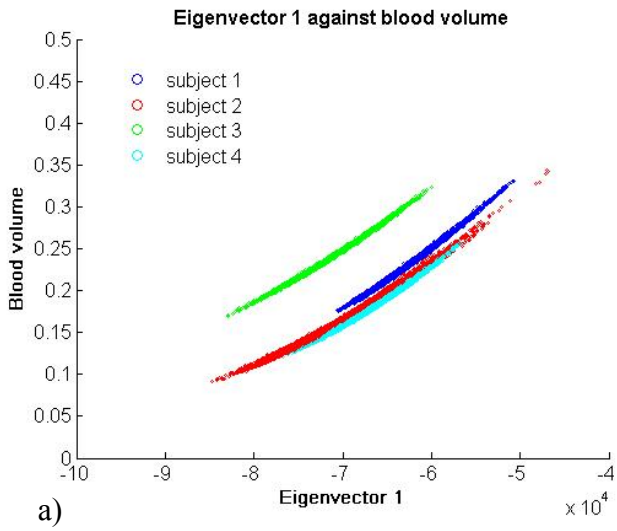
Eigenvector 1 against blood volume
subject 1
subject 2
subject 3
subject 4
Blood volume
Eigenvector 1
x 10^4
0.5
0.45
0.4
0.35
0.3
0.25
0.2
0.15
0.1
0.05
0
-10
-9
-8
-7
-6
-5
-4

a)

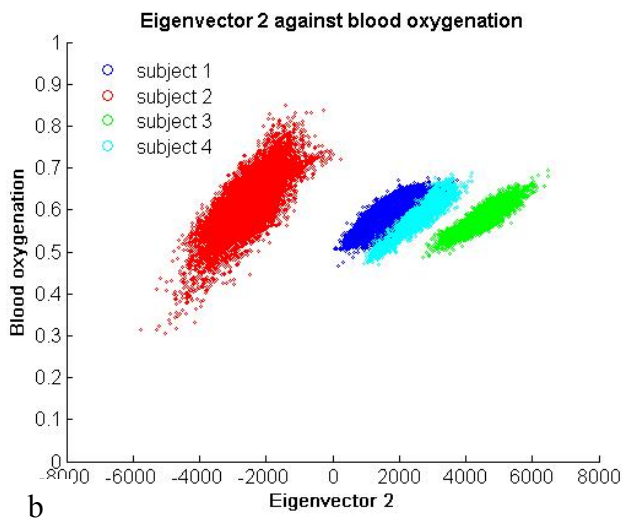
Eigenvector 2 against blood oxygenation
subject 1
subject 2
subject 3
subject 4
Blood oxygenation
Eigenvector 2
1
0.9
0.8
0.7
0.6
0.5
0.4
0.3
0.2
0.1
0
-6000
-4000
-2000
0
2000
4000
6000
8000

b